Effect of oxygenated species on pyrolysis and fuel-rich oxidation of CH_4 in the context of polygeneration: Soot optical density, CO-concentration, and temperature

Damien Nativel, Jürgen Herzler, Mustapha Fikri, and Christof Schulz
EMPI, Institute for Energy and Materials Processes – Reactive Fluids, University of Duisburg-Essen, Duisburg, Germany

1 Introduction

Polygeneration in internal combustion engines enables a variable generation of mechanical power and valuable chemicals based on reactions under fuel-rich conditions depending on the fuel/air equivalence ratio ϕ [1]. Such process can help to mitigate one of the main challenges of future energy systems – fluctuations in electricity supply and demand. Investments in devices for grid stabilization could be more economical if they have a second use [1]. In this context, IC engines can be used in ultra-rich conditions and operated in homogeneous-charge compression-ignition (HCCI) mode to overcome the limitations of spark ignition due to the low flame speed at fuel-rich conditions. To decrease the intake temperature required to initiate reactions in the available time scale, additives such as n-heptane have been used to increase the reactivity of methane [2]. The maximum mechanical power is generated at stoichiometric conditions and at $\phi = 2$, syngas (carbon monoxide and hydrogen) and less mechanical power is generated. At even more fuel-rich conditions, besides syngas also higher hydrocarbons are produced. At $\phi = 10$, about 50 % syngas and 50 % higher hydrocarbons are formed from methane and methane/additive mixtures [2]. Under such fuel-rich conditions, the reaction-induced temperature increase is low enough that the final temperature stays below the lower limit of soot formation. The disadvantage is, however, the relatively low conversion of methane at the related temperatures. To increase the conversion of the fuel by choosing less fuel-rich conditions while avoiding soot formation, oxygenated additives (e.g., diethyl ether, DEE; methanol, CH_3OH or dimethoxymethane, DMM) are of interest because they shift the onset temperature for soot formation to higher temperatures.

The influence of oxygenated components such as alcohols or ethers on soot formation has been investigated before in shock tubes [3-6], engines [7], and flames [8]. These studies showed that the presence of oxygenated components can significantly reduce the soot yield. In the study of Hong et al. [3], it is also shown that the so-called soot "bell-shaped" curve (i.e., the temperature window where soot forms) shifts to higher temperatures in the presence of oxygenated components.

Tunable diode laser absorption spectroscopy (TDLAS) is a sensitive, non-intrusive and highly selective method that can be used to detect species and measure temperature in harsh environments with high time resolution [9]. TDLAS was used in our previous work for time-resolved measurements of temperature and CO concentration in a shock tube [10, 11]. This paper aims at studying the oxidation

Correspondence to: damien.nativel@uni-due.de

of fuel-rich CH_4, CH_4/DEE, CH_4/DMM and CH_4/CH_3OH mixtures to investigate the soot behavior that limits the polygeneration process to very fuel rich mixtures. Simultaneous measurements of laser extinction at 633 nm and CO concentration and temperature using TDLAS were performed and the results were compared with chemical-kinetics based simulations [12-14].

2 Experimental details

Laser extinction, time-resolved temperature, and CO concentration profiles were measured in a shock tube behind reflected shock waves at ~5 bar in the temperature range of 1484–3200 K. The length of the driver and driven sections and the inner diameter of the shock tube are 3.6, 7.3, and 0.08 m, respectively [15, 16]. The driven section is equipped with four pressure transducers (PCB model 112A03) from which the shock velocity is obtained, which is used to calculate temperature and pressure behind the reflected shock wave using ideal shock relations (with a temperature and pressure uncertainty of ~1.5 %). One pressure transducer (PCB®) was installed at a distance of 2.0 cm from the endwall and was coated with room-temperature vulcanizing (RTV) silicone to shield the transducer from heat effects. The pressure measured with this sensor was used as input for the data processing of the time-resolved CO measurements and for the chemical kinetics simulations. Four sapphire windows were installed 2.0 cm upstream of the end wall at opposite sides of the shock tube for absorption and extinction measurements. The test mixtures were prepared manometrically in a 50-l stainless-steel mixing tank allowing to homogenize over night before use. Eight mixtures were studied and are presented in table 1.

Table 1: Composition of the investigated mixtures. All mixtures contain 20 % He and are diluted in Ar. Mixtures 5–8 contains also 1 % CO (used as target species for the pyrolysis measurements).

Nr.	Mixture (oxidation, $\phi = 5.0$)	Nr.	Mixture (pyrolysis)
Mix1	10 % CH_4 + 4.0 % O_2	Mix5	10 % CH_4
Mix2	10 % CH_4 + 1 % DEE + 5.2 % O_2	Mix6	10 % CH_4 + 1 % DEE
Mix3	10 % CH_4 + 1 % CH_3OH + 4.3 % O_2	Mix7	10 % CH_4 + 1 % CH_3OH
Mix4	10 % CH_4 + 1 % DMM + 4.8 % O_2	Mix8	10 % CH_4 + 1 % DMM

CO is used as a target species for the time-resolved temperature measurements based on two-color absorption in the infrared and He is added to accelerate vibrational relaxation of hot CO. A two-color fixed-wavelength absorption method was applied to determine time-resolved temperatures and CO concentrations. The optical setup used in this paper has been already used and validated in several publications [4-6, 10], therefore, only few details are given here. The wavelengths of two continuous-wave quantum-cascade lasers (QCL) were controlled by two QCL controllers (Arroyo instrument, QCL-6310) and were fixed at the center of two lines (v" = 0, P(8) and v" = 1, R(21) at 4.7359 and 4.5631 µm, respectively). The two laser beams were coupled into a single-mode fiber (InF3, Thorlabs) by an off-axis parabolic mirror. The two collinear beams are directed through the shock tube via two opposed sapphire windows. The transmitted beam is divided into two separate beams by a transparent quartz plate. Two bandpass filters (Spectrogon, NB-4560-135 nm and NB-4720-100 nm) in front of each detector (Vigo, PVI-3TE) were used for wavelength selection. A 25-cm absorption cell and a 20.25-m pathlength White cell filled with a gas mixture containing CO (1 %) were used to center the 4.7359-µm laser (AdTech Optics) and the 4.5631-µm laser (Hamamatsu), respectively.

Based on the Beer-Lambert law, the relationship between incident beam intensity and transmitted beam intensity can be expressed as $\left(I/I_0\right)_\nu = \exp\left(-pS(T)lx\varphi(\nu)\right)$, with p is the pressure, atm, $S(T)$ in $cm^{-2}bar^{-1}$ is the line strength at a certain temperature, l is the inner diameter of the shock tube and thus the absorption path length, x is the species mole fraction, $\varphi(\nu)$ is the line shape that is assumed here to follow

a Voigt function. The ratio $R(T)$ of the peak absorbance at the line center of both transitions is only a function of the temperature and the temperature can be calculated according to eq. 2:

$$T(R) = \left[\ln \frac{R(T)}{R(T_0)} \cdot \frac{k_B}{hc} \cdot \frac{1}{E_2'' - E_1''} + \frac{1}{T_0} \right]^{-1} \quad (2)$$

T_0 is the reference temperature (296 K), E'' is the lower-state energy of the transition, h, c, k_B are the Planck constant, speed of light, and the Boltzmann constant, respectively. The line strengths of the P8 and R21 lines are taken from HITEMP database [17]. Collisional broadening coefficient and broadening index was taken from Ren et al. [10, 18]. Temperature and CO concentration profiles were calculated in an iterative way as described in our previous publications [10, 11].

Soot formation was observed by recording extinction of 633-nm radiation from a HeNe laser with an integrating sphere (Thorlabs, model IS236A-4) equipped with a 630±10-nm interference filter attached to a photodiode (model SM05PD1B) through side windows in the shock tube, 20 mm away from the end flange. The measurements were evaluated using the approach of the normalized optical densities D_{633nm} presented in [19]. The normalized optical density is given as $D_{633nm} = \ln(I_0/I)/([C]l)$, with l is the absorption length, I_0 and I are the incident and transmitted signal respectively, and [C] is the total carbon concentration related to soot in the respective mixture.

Figure 1 presents typical temporal profiles of D_{633nm}. The optical density at a fixed time of 3.0 ms was chosen because the profiles reach the plateau value within the test time. This particular time was set according to the evolution of the pressure behind the reflected shock wave. Indeed, at a time of 3.0 ms, conditions at the cooling phase were observed for all investigated mixtures (see pressure profile in Figure 1).

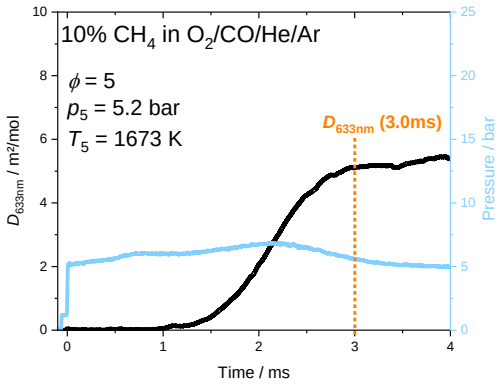

Figure 1: Pressure and temporal profiles of D_{633nm}.

3 Results and discussion

Figure 2 shows the measured temperature profiles during the oxidation of the investigated mixtures and also the predictions of three detailed kinetics mechanisms [12-14, 20]. The simulation was performed with Chemical Workbench [21] using a "specified-pressure" reactor model with implementation of the measured pressure profile for non-reactive mixture. For all mixtures, a temperature rises due to the oxidation of the fuel is observed before soot formation begins analogous to previous work [19]. The soot formation therefore proceeds at higher temperatures exceeding T_5. Therefore, an accurate knowledge of the temperature profile during oxidation is necessary for soot modeling. For pure CH_4 (Figure 2a), good agreement between experiment and simulation is observed with the Aramco 3.0 mechanism [13] and the Fikri et al. [14] mechanism. Also, good agreement is observed with Yasunaga et al. mechanism [12] at higher temperatures (1706 and 1802 K). For CH_4/DEE (Figure 2b), no simulation was performed with Aramco 3.0 [13] since DEE is not included in this mechanism. A too

slow prediction is noticed for both mechanisms (Fikri et al. [14] and Yasunaga et al. [12]) even if a better agreement is reached for the Yasunaga et al. [12] mechanisms at higher temperatures. Concerning the mixture with CH_3OH as additive (Figure 2c), the experiments were compared with the predictions of the Aramco3.0 mechanism and good agreement is observed in the whole temperature range. Figure 2d shows the temperature results for Mix4 with DMM as additive. A good agreement between the experimental and the simulation results with a slight deviation at high temperature is observed. For Mix4, only the mechanism of Jacobs et al. [20] was used since DMM was not presented in the other tested mechanisms.

The CO concentration profiles are also presented in Figure 2 together with the simulations with the aforementioned mechanisms. For pure CH_4 (Figure 2e), the best agreement is achieved with the Fikri et al. [14] and Aramco3.0 [13] mechanisms even if at the lowest temperature, the three tested mechanisms predict a too slow formation of CO. For CH_4/DEE (Figure 2f), the two tested mechanisms predict a too slow CO formation. When the plateau of CO formation is reached, the Yasunaga et al. [12] mechanism yields too high CO concentrations. This observation requires further analysis to understand the different shapes of experimental and simulated profiles. For CH_4/CH_3OH (Figure 2g), the simulation is slightly too fast but overall good agreement is achieved similarly to the corresponding temperature measurements. Generally, slightly too high CO concentrations are predicted. The temperature and CO profiles show that methanol and especially DEE and DMM leads to a faster ignition. Considering the Mix4 with DMM (Figure 2h), good agreement of the CO increase is observed except at low temperature.

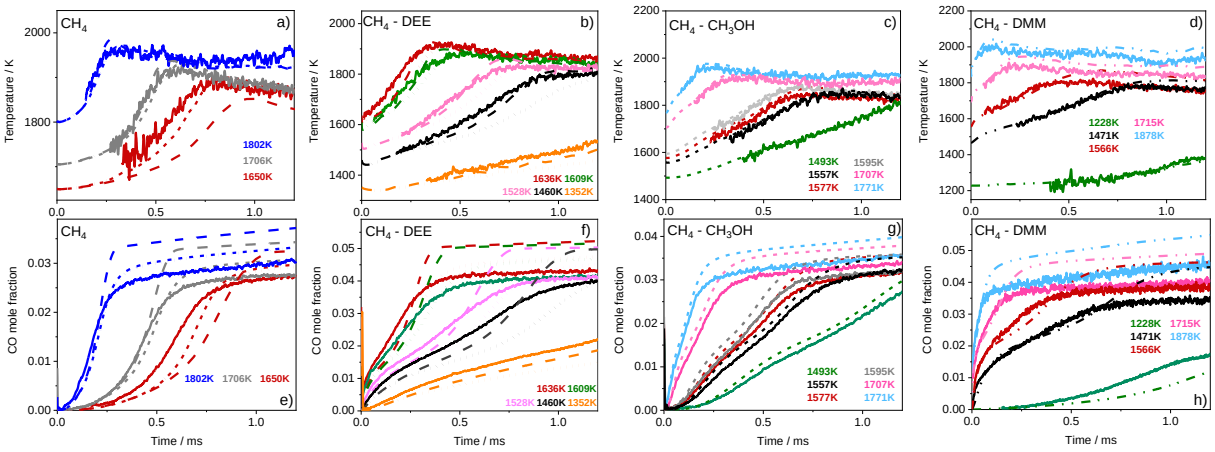

Figure 2: Top: Temperature profiles measured in different mixtures. Bottom: CO concentration profiles: a, e) Mix1; b, f) Mix2; c, g) Mix3, and d, h) Mix4. All the experiments are compared with simulations based on the mechanisms of Yasunaga et al. [12] (dashed lines, frames a, b, e, f), Aramco 3.0 [13] (short dashed lines, frames a, c, e, g), Fikri et al. [14] (short dotted lines, frames a, b, e, f) and Jacobs et al. [20] (short dashed-dot-dot lines, frames d, h)

Figure 3 shows the optical density results together with the simulation results. For the optical density simulation, the method presented in the previous publication from our group was used [4, 6]. All the simulation were performed with the detailed kinetics mechanism of Nobili et al. [22]. Experimentally, a characteristic "bell-shaped" curve as observed in the literature [3, 19] is found. Concerning the oxidation results, for the reference mixture Mix1, the maximum optical density is reached at $T \approx 1700$ K with a value of $D_{633nm} \approx 5$ m^2/mol. DEE increases the soot yield slightly and lower soot yield is reached with CH_3OH compared to Mix1. The formation of soot is shifted towards lower temperature when using additives. For instance, taking the CH_4 mixture at $T = 1590$ K as a reference, we notice that soot is formed at a temperature ~40 K lower for the mixture with CH_3OH as additive and at a temperature ~100 K lower for the mixture with DEE as additive. This can be explained by the faster ignition of the mixtures with additives. For DMM, a decrease of the soot yield by ~25 % (at the maximum) is observed

compared to the reference mixture. Very good agreement between experiment and simulation is observed and the influence of additives is reproduced by the simulation.

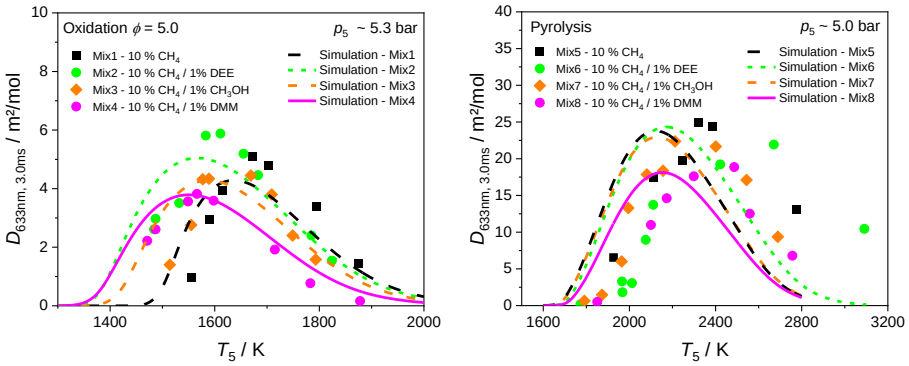

Figure 3: Optical density D_{633nm} measured at t = 3.0 ms. Left: Oxidation. Right: Pyrolysis.

A soot reducing effect of DMM on the soot yield is also observed on the pyrolysis plot (Figure 3, right) with a 20 % decrease of the soot yield at the maximum compared to the reference mixture. The simulation of the pyrolysis results is also in good agreement with the experimental results except a shift of about 200 K towards lower temperatures of the simulations. A very good prediction of the soot reducing effect of DMM is observed.

4 Conclusions

The pyrolysis and the oxidation of fuel rich CH_4 mixtures (ϕ = 5) and the influence of three oxygenated additives (diethyl ether, methanol and dimethoxymethane) on soot formation between 1484–3200 K at ~5 bar were studied in a shock tube. Temperature and CO concentrations were determined as a function of time after the arrival of the reflected shock wave using IR absorption measurements on the fundamental vibrational transitions of CO (P8 and R21). The experimental results were compared to the predictions of four detailed kinetics models (Yasunaga et al. [12], Aramco3.0 [13], Fikri et al. [14] and Jacobs et al. [20]). Simulations with the Aramco3.0 mechanism showed very good agreement for the pure CH_4 and CH_4/CH_3OH experiments whereas the predictions from the mechanism of Yasunaga et al. agree quite well with the CH_4/DEE experiments. Laser-induced extinction experiments were also simultaneously performed to measure the soot yield. The major result of these experiments is that DMM decreases the soot yield, DEE increases the soot yield and that a slightly lower soot yield is reached with CH_3OH compared to pure CH_4. The formation of soot is shifted towards lower temperature when using DMM, CH_3OH or DEE as additives. The simulation of the soot yield results with the Nobili et al. mechanism [22] presents an overall good agreement with the experimental results. In future work, the influence of additional oxygenate additives will be investigated and analyzed whether they are better suited to prevent soot formation at very fuel-rich conditions in polygeneration processes and further kinetics analysis will be performed to understand the effect of these additives on the change in the initial routes of soot formation.

5 Acknowledgements

Financial support by the German Research Foundation within the framework of the DFG research unit FOR 1993 “Multifunctional conversion of chemical species and energy” (Project number 229243862) is gratefully acknowledged.

References

[1] Atakan B, Kaiser SA, Herzler J, Porras S, Banke K, Deutschmann O, Kasper T, Fikri M, Schießl R, Schröder D, Rudolph C, Kaczmarek D, Gossler H, Drost S, Bykov V, Maas U, Schulz C. (2020). Flexible energy conversion and storage via high-temperature gas-phase reactions: The piston engine as a polygeneration reactor. Renew. Sust. Energ. Rev. 133: 110264.

[2] Herzler J, Sakai Y, Fikri M, Schulz C. (2019). Shock-tube study of the ignition and product formation of fuel-rich CH_4/air and CH_4/additive/air mixtures at high pressure. Proc. Combust. Inst. 37: 5705.

[3] Hong Z, Davidson DF, Vasu SS, Hanson RK. (2009). The effect of oxygenates on soot formation in rich heptane mixtures: A shock tube study. Fuel 88: 1901.

[4] Nativel D, Herzler J, Krzywdziak S, Peukert S, Fikri M, Schulz C. (2022). Shock-tube study of the influence of oxygenated additives on benzene pyrolysis: Measurement of optical densities, soot inception times and comparison with simulations. Combust. Flame 243: 111985.

[5] Nativel D, Peukert S, Herzler J, Drakon A, Korshunova M, Mikheyeva E, Eremin A, Fikri M, Schulz C. (2022). Shock-tube study on the influence of oxygenated co-reactants on ethylene decomposition under pyrolytic conditions. Proc. Combust. Inst. DOI: 10.1016/j.proci.2022.07.209

[6] Nativel D, Shao C, Cooper SP, Petersen EL, Schulz C, Fikri M, Peukert S. (2023). Impact of methanol and butanol on soot formation in gasoline surrogate pyrolysis: A shock-tube study. J. Phys. Chem. A. DOI: 10.1021/acs.jpca.2c06599

[7] Zubel M, Heuser B, Pischinger S. (2017). 1-Octanol tailor-made fuel for lower soot emissions. MTZ worldwide. 78: 58.

[8] Russo C, D'Anna A, Ciajolo A, Sirignano M. (2019). The effect of butanol isomers on the formation of carbon particulate matter in fuel-rich premixed ethylene flames. Combust. Flame 199: 122.

[9] Sun K, Sur R, Chao X, Jeffries JB, Hanson RK, Pummill RJ, Whitty KJ. (2013). TDL absorption sensors for gas temperature and concentrations in a high-pressure entrained-flow coal gasifier. Proc. Combust. Inst. 34: 3593.

[10] He D, Nativel D, Herzler J, Jeffries JB, Fikri M, Schulz C. (2020). Laser-based CO concentration and temperature measurements in high-pressure shock-tube studies of n-heptane partial oxidation. Appl. Phys. B. 126: 142.

[11] He D, Shi L, Nativel D, Herzler J, Fikri M, Schulz C. (2020). CO-concentration and temperature measurements in reacting CH_4/O_2 mixtures doped with diethyl ether behind reflected shock waves. Combust. Flame 216: 194.

[12] Yasunaga K, Simmie JM, Curran HJ, Koike T, Takahashi O, Kuraguchi Y, Hidaka Y. (2011). Detailed chemical kinetic mechanisms of ethyl methyl, methyl tert-butyl and ethyl tert-butyl ethers: The importance of uni-molecular elimination reactions. Combust. Flame 158: 1032.

[13] Zhou C-W, Li Y, Burke U, Banyon C, Somers KP, Ding S, Khan S, Hargis JW, Sikes T, Mathieu O, Petersen EL, AlAbbad M, Farooq A, Pan Y, Zhang Y, Huang Z, Lopez J, Loparo Z, Vasu SS, Curran HJ. (2018). An experimental and chemical kinetic modeling study of 1,3-butadiene combustion: Ignition delay time and laminar flame speed measurements. Combust. Flame 197: 423.

[14] Fikri M, Sakai Y, Herzler J, Schulz C. (2017). Experimental and numerical study of the ignition delay times of primary reference fuels containing diethylether. Proceedings of the 26th International Colloquium on the Dynamics of Explosions and Reactive Systems. Paper Nr. 957.

[15] Fikri M, Makeich A, Rollmann G, Schulz C, Entel P. (2008). Thermal decomposition of trimethylgallium $Ga(CH_3)_3$: A shock-tube study and first-principles calculations. J. Phys. Chem. A. 112: 6330.

[16] Nativel D, Cooper SP, Lipkowicz T, Fikri M, Petersen EL, Schulz C. (2020). Impact of shock-tube facility-dependent effects on incident- and reflected-shock conditions over a wide range of pressures and Mach numbers. Combust. Flame. 217: 200.

[17] Rothman LS, Gordon IE, Barber RJ, Dothe H, Gamache RR, Goldman A, Perevalov VI, Tashkun SA, Tennyson J. (2010). HITEMP, the high-temperature molecular spectroscopic database. J. Quant. Spectrosc. Rad. Transf. 111: 2139.

[18] Ren W, Farooq A, Davidson DF, Hanson RK. (2012). CO concentration and temperature sensor for combustion gases using quantum-cascade laser absorption near 4.7 μm. Appl. Phys. B. 107: 849.

[19] Drakon A, Eremin A, Mikheyeva E, Shu B, Fikri M, Schulz C. (2018). Soot formation in shock-wave-induced pyrolysis of acetylene and benzene with H_2, O_2, and CH_4 addition. Combust. Flame 198: 158.

[20] Jacobs S, Döntgen M, Alquaity ABS, Kopp WA, Kröger LC, Burke U, Pitsch H, Leonhard K, Curran HJ, Heufer KA. (2019). Detailed kinetic modeling of dimethoxymethane. Part II: Experimental and theoretical study of the kinetics and reaction mechanism. Combust. Flame 205: 522.

[21] Deminsky M, Chorkov V, Belov G, Cheshigin I, Knizhnik A, Shulakova E, Shulakov M, Iskandarova I, Alexandrov V, Petrusev A, Kirillov I, Strelkova M, Umanski S, Potapkin B. (2003). Chemical Workbench—integrated environment for materials science. Comp. Mater. Sci. 28: 169.

[22] Nobili A, Cuoci A, Pejpichestakul W, Pelucchi M, Cavallotti C, Faravelli T. (2022). Modeling soot particles as stable radicals: a chemical kinetic study on formation and oxidation. Part I. Soot formation in ethylene laminar premixed and counterflow diffusion flames. Combust. Flame 243: 112073.